Nanoscale

PAPER

View Article Online
View Journal | View Issue

Cite this: *Nanoscale*, 2023, **15**, 6954

Stabilizing $FASnI_3$-based perovskite light-emitting diodes with crystallization control†

Guoling Zhang,‡ Shiyu Xing,‡ Xuhui Cao, Baodan Zhao* and Dawei Di *

Received 11th January 2023,
Accepted 25th March 2023

DOI: 10.1039/d3nr00177f

rsc.li/nanoscale

The toxicity of lead presents a critical challenge for the application of perovskite optoelectronics. Lead-free perovskite solar cells were achieved with formamidinium tin iodide ($FASnI_3$) perovskites, exhibiting decent power-conversion efficiencies (PCEs) of up to 14%, with >98% of the initial PCE retained after 3000 h of storage. However, when employed in light-emitting applications, $FASnI_3$-based perovskite LEDs (PeLEDs) show limited stability, with T_{50} lifetimes of up to 0.25 h at 10 mA cm^{-2}. Here, we improve the stability of $FASnI_3$-based PeLEDs through the inclusion of a two-dimensional precursor phenethylamine iodide (PEAI), allowing controlled crystallization of the mixed-dimensional perovskite emitters. The density of defects is found to be reduced, accompanied by the suppression of oxidation from Sn^{2+} to Sn^{4+}. Using an optimized perovskite composition, we achieve an EQE of 1.5% (a ~10-fold improvement over the control devices), a maximum radiance of 145 W sr^{-1} m^{-2}, and a record-long T_{50} lifetime of 10.3 h at 100 mA cm^{-2} for $FASnI_3$-based PeLEDs. Our results illuminate an alternative path toward lead-free PeLED applications.

1. Introduction

Metal halide perovskites have emerged as a competitive candidate for next-generation display and lighting technologies. Their excellent optoelectronic properties enabled a massive progress in perovskite light-emitting diode (PeLED) applications,[1–13] with external quantum efficiencies (EQEs) exceeding 20% for PeLEDs with various colors[3–9] and recent breakthroughs in operational stability.[8,9] However, the toxicity of lead-based perovskite materials has been considered an ongoing challenge towards practical applications. To address this issue, considerable attention has been paid to Pb-free and eco-friendly alternatives, including tin (Sn),[14–16] germanium (Ge),[17] copper (Cu),[18,19] antimony (Sb)[20] and bismuth (Bi)[21]-based perovskite emitters. Among these low-toxicity perovskite materials, Sn-based perovskites are considered as one of the most promising eco-friendly alternatives, as Sn^{2+} shows an ionic radius and outer electronic structure comparable to that of Pb^{2+}.[22–24] Recently, it was reported that $FASnI_3$-based perovskite solar cells showed power conversion efficiencies (PCEs) of up to 14%,[25,26] representing the highest PCE reported among all lead-free perovskite solar cells. The cells retained >98% of their initial PCE after 3000 h of storage. These results indicate the potential applications of $FASnI_3$ perovskite in other lead-free optoelectronic devices, including PeLEDs. While $FASnI_3$-based PeLEDs have recently reached EQEs of over 5%,[14] their operational stability remains poor, showing T_{50} lifetimes of 0.25 h at 10 mA cm^{-2}. The performance of $FASnI_3$-based PeLEDs may be limited by two factors. First, the rapid crystallization process, resulting from the fast reaction rates of SnI_2 and FAI, may lead to a high density of grain boundary defects and poor surface morphology.[24,27,28] Secondly, the chemical instability due to Sn^{2+}/Sn^{4+} oxidation could result in the formation of traps, leading to unsatisfactory efficiency and stability.[17,22]

In this work, we show that the inclusion of PEAI in the $FASnI_3$ perovskite precursor has a substantial impact on the crystallization process. Using a range of structural and optical characterizations, we demonstrate that the PEAI incorporation generally improves the crystallinity and suppresses the oxidation of the lead-free perovskite emitters. We fabricate $FASnI_3$-based PeLEDs with improved stability. The champion device shows a T_{50} lifetime of 10.3 h under a high current density of 100 mA cm^{-2}, representing a step forward for the operational stability of $FASnI_3$-based PeLEDs (previous T_{50} record: 0.25 h at 10 mA cm^{-2}).[14]

2. Results and discussion

The perovskite precursor solution was prepared by dissolving FAI, PEAI and SnI_2 at a molar ratio of $(1 - x\%) : x\% : 1$ $(0 \leq x \leq$

State Key Laboratory of Extreme Photonics and Instrumentation, College of Optical Science and Engineering; International Research Center for Advanced Photonics, Zhejiang University, Hangzhou, 310027, China. E-mail: daweidi@zju.edu.cn, baodanzhao@zju.edu.cn

†Electronic supplementary information (ESI) available. See DOI: https://doi.org/10.1039/d3nr00177f

‡These authors contributed equally to this work.

100) (Methods). The perovskite samples were formed following spin-coating and annealing. For simplicity, the perovskite samples prepared from precursor with x% of PEAI were named as "x% PEAI". The "control" samples correspond to samples without any PEAI inclusion (x = 0). The control sample exhibits X-ray diffraction (XRD) peaks at 14.1°, 24.4°, 28.3°, 31.7°, 40.4° and 43.0°, which are assigned to the crystallographic planes of (100), (102), (200), (122), (222), and (213) of the orthorhombic phase of $FASnI_3$ (Fig. 1a).[25,29] While the 5–20% PEAI samples show two strong diffraction peaks at 14.1° and 28.3°, suggesting the presence of 3D $FASnI_3$ and improved crystallinity (Fig. S1†).[30] The crystallization process may be affected by the π–π staking interactions at the benzene headgroup of PEAI, leading to a more preferential growth of the perovskite crystallites.[31] A weak diffraction peak at 4° corresponding to 2D perovskite could be observed for the 20% PEAI samples (Fig. S1†). Further, the presence of low-dimensional phases in the 5% and 10% PEAI samples can be identified from the transient absorption measurements (Fig. S2†). However, as shown in 40% and 80% PEAI samples, the decreased peak intensity and emergence of the low-dimensional peaks (<10°) indicate that excessive PEAI impedes the formation of $FASnI_3$ perovskite, forming a larger fraction of low-dimensional phases.

The surface morphology of the samples was studied using scanning electron microscopy (SEM) (Fig. 1b–f). The control sample shows a rough and porous surface structure. Overall, PEAI has a significant effect on the surface morphology of perovskite films (Fig. 1c–f). A 5% PEAI inclusion was sufficient for increasing the grain size and reduce the density of pinholes. At a PEAI inclusion of 10%, the uniformity of the samples appears to reach an optimum. However, an excessive amount of PEAI reduces the coverage of the perovskite films, as was found for the 20%, 40% and 80% PEAI samples (Fig. 1e, f and Fig. S3†). The smaller crystallites of the 40% and 80% PEAI samples (Fig. 1f and Fig. S3†) may be attributed to the formation of low-dimensional perovskite phases, consistent with their XRD patterns (Fig. 1a).

To characterize the optical properties of the samples, photoluminescence (PL) and absorption measurements were carried out. When the molar ratio of PEAI is ≤10%, the samples show very similar absorption edge near 900 nm, corresponding to the band edge of bulk $FASnI_3$ (Fig. 2a). When the molar ratio of PEAI increases to 20%, the absorption edge shifts to shorter wavelength at 875 nm, which may be related to the quantum confinement effects in low-dimensional phases. The absorbance of the perovskite samples near the band edge gradually decrease with the increase of PEAI inclusion, which may be attributed to smaller film thicknesses (Table S1†). Further increasing the content of PEAI, a new excitonic absorption peak appears at 670 nm, corresponding to the low-dimensional phase of n = 2, consistent with the XRD results.[31] Similar effects can be seen from the PL results (Fig. 2b). A small blueshift is observed in the 20% PEAI sample, and the emission from low-dimensional phases become pronounced for the 40% and 80% PEAI samples. The PL quantum efficiencies (PLQEs) of the samples reach maximum at a PEAI molar fraction of 10%, while further increasing the PEAI content reduces the PLQE (Fig. 2c).

Transient PL and space-charge-limited current (SCLC) measurements[32,33] were performed to investigate the effects of

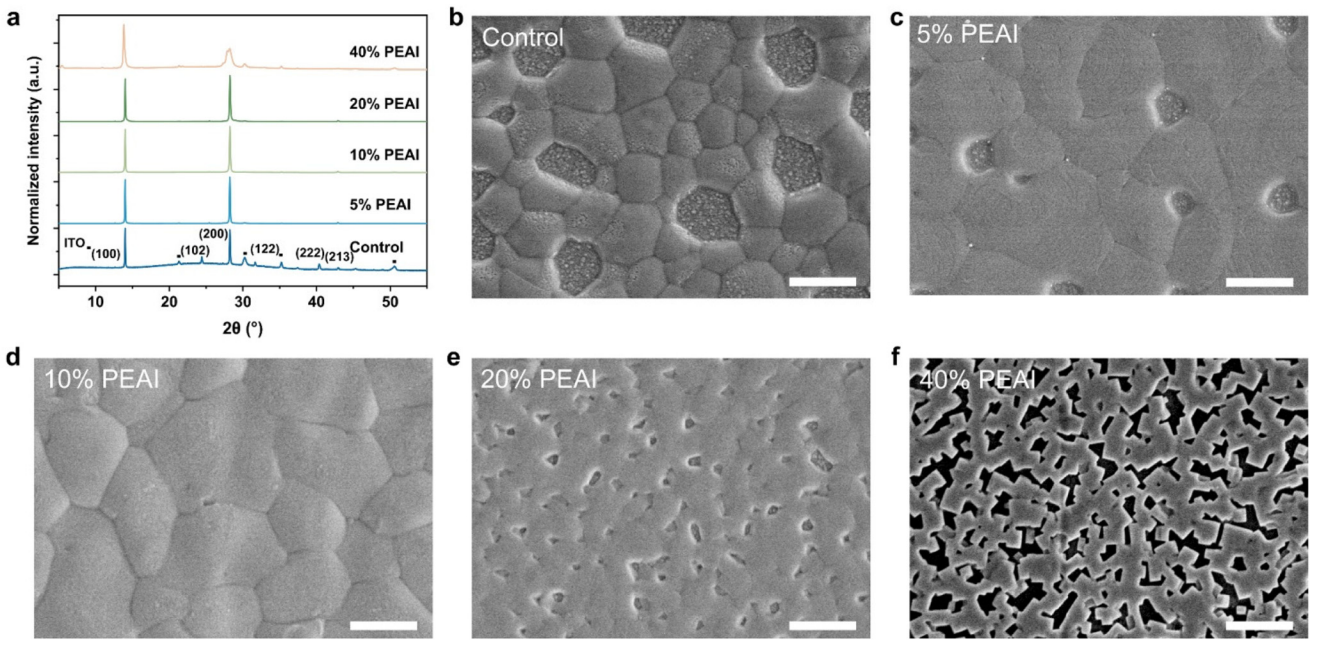

Fig. 1 Structural and morphological characteristics of the perovskite films. (a) The XRD patterns of the perovskite samples (control, 5% PEAI, 10% PEAI, 20% PEAI, 40% PEAI) with a MgF_2 capping layer. (b–f) The SEM images of the perovskite samples (control, 5% PEAI, 10% PEAI, 20% PEAI, 40% PEAI) (scale bars: 2 μm).

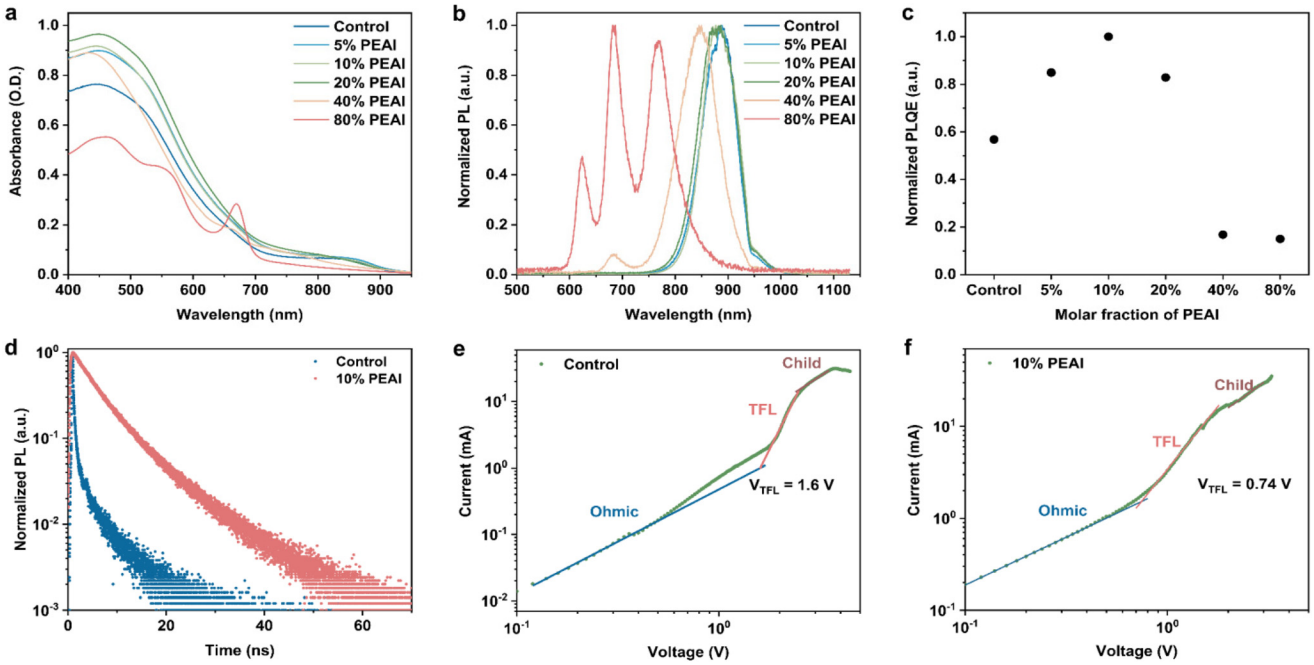

Fig. 2 Optical characteristics of the perovskite samples. (a) UV–vis absorption and (b) photoluminescence (PL) spectra. (c) Normalized PLQE of the lead-free perovskite samples with different molar fraction of PEAI (control, 5% PEAI, 10% PEAI, 20% PEAI, 40% PEAI, 80% PEAI). (d) Transient PL kinetics of the control and 10% PEAI samples. Excitation fluence: 160 nJ cm^{-2}, at 400 nm. (e and f) SCLC measurements for the control and 10% PEAI samples (device structure: ITO/TPBi/perovskite/TPBi/LiF/Al).

traps in the samples. The effective PL lifetime (the time required for the PL intensity to reduce to 1/*e* of its initial intensity) of the pristine $FASnI_3$ (control) sample is 0.2 ns (Fig. 2d), while the 10% PEA sample shows a much longer lifetime of 5.5 ns, indicating a reduced density of traps. This is consistent with the SCLC measurements (Fig. 2f, g and Fig. S4†), showing a reduced trap-filled limited voltage (V_{TFL}) of ~0.74 V for the 10% PEAI sample, in contrast to a V_{TFL} of ~1.60 V for the control sample.

X-ray photoelectron spectroscopy (XPS) measurements were carried out to study the redox processes in the samples. Sn 3d spectra of the control and 10% PEAI samples were analyzed to trace the presence of Sn^{2+} and Sn^{4+} (Fig. 3a and b). The fraction of Sn^{4+} was estimated from the areas under the curves.[34,35] The fraction of Sn^{4+} in the control samples is 60.1% (Fig. 3a). This value reduces to 11.4% for the 10% PEAI samples, indicating the incorporation of PEAI may help suppressing the oxidation of Sn^{2+} within the perovskite films.[31,36–38] Moreover, the peaks associated with Sn^{2+} shift to lower binding energies (from 486.72 eV to 486.25 eV), indicating the decreased cationic charges on Sn^{2+} with the inclusion of PEAI, in agreement with the inhibited oxidation of Sn^{2+}. The inhibition of oxidation of Sn^{2+} may be attributed to the improved crystallinity of the perovskite samples and the

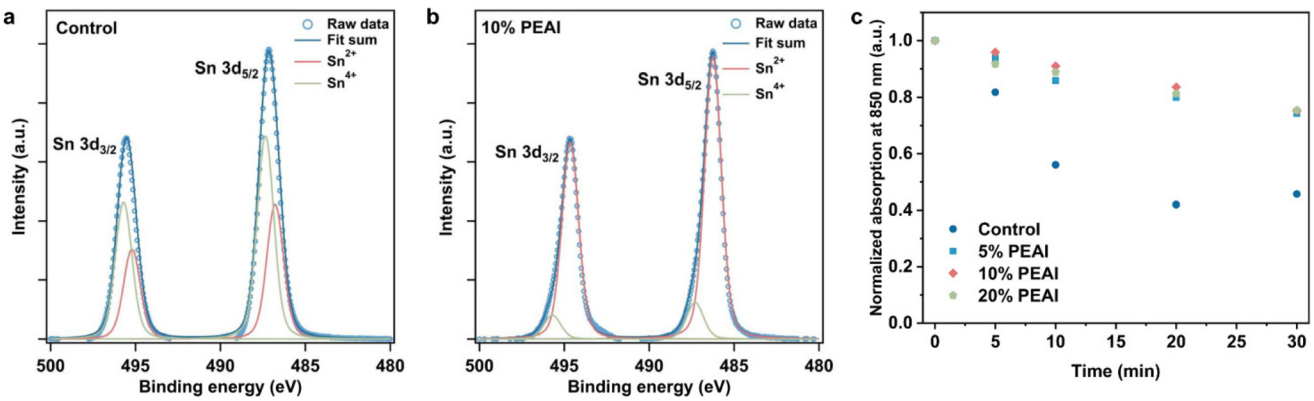

Fig. 3 XPS and absorption analyses for the perovskite samples. (a and b) Sn 3d spectra of the control and the 10% PEAI perovskite samples. (c) The evolution of the absorption strength at ~850 nm of the perovskite samples exposed in air (temperature: 20 ± 5 °C, humidity: 70%).

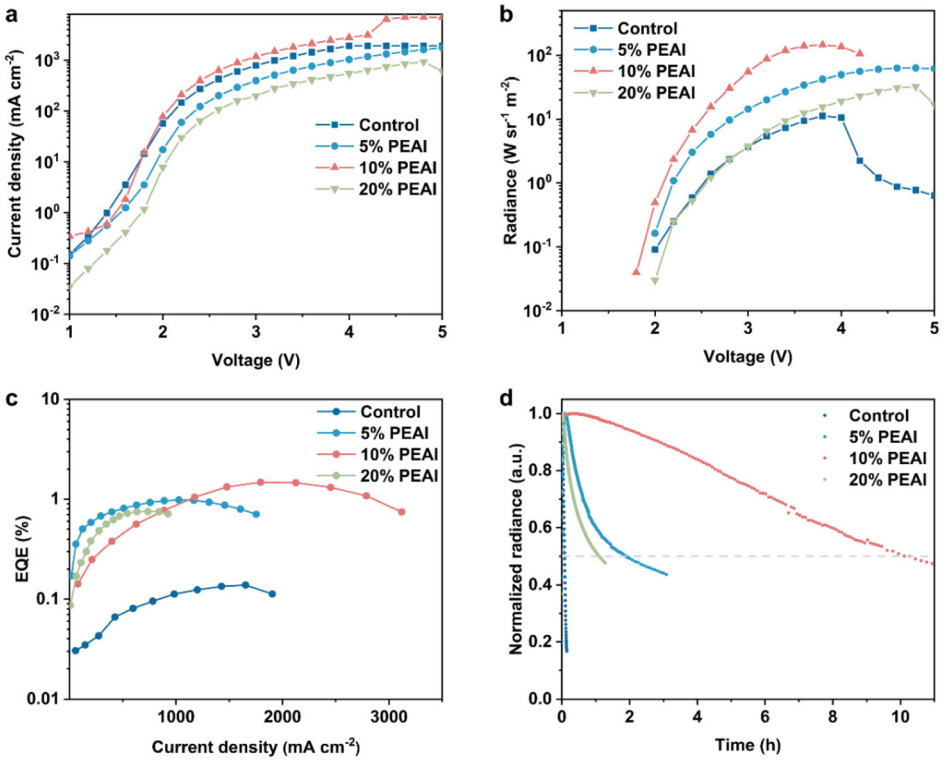

Fig. 4 Device characterization for $FASnI_3$-based PeLEDs with different PEAI molar fractions. (a) Current density–voltage characteristics. The sudden increase of current density of the 10% PEAI device may be attributed to thermal accumulation under large current densities (~3 A cm^{-2}), leading to device breakdown. (b) Radiance–voltage curves. (c) EQE–current density curves of the PeLEDs. (d) EL lifetime tests for PeLEDs (under a current density of 100 mA cm^{-2}).

inclusion of two-dimensional phases with higher oxygen and humidity resistance.[38–43] The suppressed oxidation of Sn^{2+} may help preventing the formation of Sn^{2+} vacancy defects, consistent with the transient PL and SCLC results. Further, the oxidation processes could be linked to the evolution of the absorption spectra over time for samples exposed in air (Fig. S6†). For the control sample, the absorption at ~850 nm clearly reduced over 30 min (Fig. 3c), in line with its poor resistance to oxidation.[44] The sample appeared to be more transparent over time (Fig. S6,† inset). In comparison, the 10% PEAI sample showed a slower reduction of absorption over 30 min, indicating improved stability in air.

We fabricated PeLEDs with a device structure of ITO/PEDOT:PSS/perovskite/TPBi/LiF/Al. The radiance and EQEs of the 5% and 10% PEAI-based devices showed considerable improvements over the control devices (Fig. 4a–c). The 10% PEAI-based devices reached a peak EQE of 1.5% (a ~10-fold improvement over that of the control) at a high current density of ~1800 mA cm^{-2}, and a high maximum radiance of 145 W sr^{-1} m^{-2}. The EL performance reduced for a PEAI inclusion of 20%. All PeLEDs with PEAI incorporation showed similar EL spectra with that of the pristine $FASnI_3$ control devices, suggesting that radiative recombination in the mixed-dimensional perovskite emitters primarily occurs in the 3D $FASnI_3$ regions (Fig. S7†). Importantly, these devices showed decent EL stability in a N_2 glovebox (Fig. 4d). Under a high constant current density of 100 mA cm^{-2}, the devices with 10% PEAI inclusion showed the longest operational lifetime (T_{50}) of 10.3 h, representing a record for $FASnI_3$-based PeLEDs (previous T_{50} record: 0.25 h at 10 mA cm^{-2}).[14] The T_{50} results are comparable with the best-performing lead-free PeLEDs.[16]

3. Conclusion

In summary, we have demonstrated that the operational stability of $FASnI_3$-based PeLEDs can be improved by introducing an appropriate fraction (~10%) of PEAI in the perovskite precursor. The PEAI inclusion allows controlled crystallization processes that lead to uniform perovskite emissive layers with improved crystallinity. It also suppresses the detrimental oxidation of Sn^{2+} to Sn^{4+}, reducing the density of traps and improving the chemical stability of the lead-free perovskite emitters. The lead-free PeLEDs we fabricated showed a peak EQE of 1.5%, and a maximum radiance of 145 W sr^{-1} m^{-2} with a small efficiency roll-off. Under a high constant current density of 100 mA cm^{-2}, the PeLEDs reached a lifetime (T_{50}) of 10.3 h, representing a record for $FASnI_3$-based PeLEDs. Our work highlights an alternative approach for the realization of lead-free PeLEDs with high operational stability.

Contributions

G.Z. and S.X. planned the project under the guidance of D.D. and B.Z. G.Z. fabricated and characterized the LEDs. G.Z. and S.X. carried out the data analysis. X.C. and S.X. carried out the steady-state PL and TCSPC studies. G.Z. and S.X. wrote the manuscript, which was revised by D.D. and B.Z. All authors contributed to the work and commented on the paper.

Conflicts of interest

The authors declare no competing interests.

Acknowledgements

This work was supported by the National Natural Science Foundation of China (NSFC) (62005243, 62274144, 61975180), Kun-Peng Programme of Zhejiang Province (D. D.), the Natural Science Foundation of Zhejiang Province (LR21F050003) (B. Z.), the Fundamental Research Funds for the Central Universities, and Zhejiang University Education Foundation Global Partnership Fund. The authors acknowledge the administrative support from Minhui Yu and Yuzhen Zhao.

References

1 Z. K. Tan, R. S. Moghaddam, M. L. Lai, P. Docampo, R. Higler, F. Deschler, M. Price, A. Sadhanala, L. M. Pazos, D. Credgington, F. Hanusch, T. Bein, H. J. Snaith and R. H. Friend, *Nat. Nanotechnol.*, 2014, **9**, 687–692.
2 Y. Cao, N. Wang, H. Tian, J. Guo, Y. Wei, H. Chen, Y. Miao, W. Zou, K. Pan, Y. He, H. Cao, Y. Ke, M. Xu, Y. Wang, M. Yang, K. Du, Z. Fu, D. Kong, D. Dai, Y. Jin, G. Li, H. Li, Q. Peng, J. Wang and W. Huang, *Nature*, 2018, **562**, 249–253.
3 K. Lin, J. Xing, L. N. Quan, F. P. G. de Arquer, X. Gong, J. Lu, L. Xie, W. Zhao, D. Zhang, C. Yan, W. Li, X. Liu, Y. Lu, J. Kirman, E. H. Sargent, Q. Xiong and Z. Wei, *Nature*, 2018, **562**, 245–248.
4 T. Chiba, Y. Hayashi, H. Ebe, K. Hoshi, J. Sato, S. Sato, Y.-J. Pu, S. Ohisa and J. Kido, *Nat. Photonics*, 2018, **12**, 681–687.
5 B. Zhao, S. Bai, V. Kim, R. Lamboll, R. Shivanna, F. Auras, J. M. Richter, L. Yang, L. Dai, M. Alsari, X.-J. She, L. Liang, J. Zhang, S. Lilliu, P. Gao, H. J. Snaith, J. Wang, N. C. Greenham, R. H. Friend and D. Di, *Nat. Photonics*, 2018, **12**, 783–789.
6 W. Xu, Q. Hu, S. Bai, C. Bao, Y. Miao, Z. Yuan, T. Borzda, A. J. Barker, E. Tyukalova, Z. Hu, M. Kawecki, H. Wang, Z. Yan, X. Liu, X. Shi, K. Uvdal, M. Fahlman, W. Zhang, M. Duchamp, J.-M. Liu, A. Petrozza, J. Wang, L.-M. Liu, W. Huang and F. Gao, *Nat. Photonics*, 2019, **13**, 418–424.
7 Z. Liu, W. Qiu, X. Peng, G. Sun, X. Liu, D. Liu, Z. Li, F. He, C. Shen, Q. Gu, F. Ma, H. L. Yip, L. Hou, Z. Qi and S. J. Su, *Adv. Mater.*, 2021, **33**, e2103268.
8 B. Guo, R. Lai, S. Jiang, L. Zhou, Z. Ren, Y. Lian, P. Li, X. Cao, S. Xing, Y. Wang, W. Li, C. Zou, M. Chen, Z. Hong, C. Li, B. Zhao and D. Di, *Nat. Photonics*, 2022, **16**, 637–643.
9 J. S. Kim, J. M. Heo, G. S. Park, S. J. Woo, C. Cho, H. J. Yun, D. H. Kim, J. Park, S. C. Lee, S. H. Park, E. Yoon, N. C. Greenham and T. W. Lee, *Nature*, 2022, **611**, 688–694.
10 J. Chen, J. Wang, X. Xu, J. Li, J. Song, S. Lan, S. Liu, B. Cai, B. Han, J. T. Precht, D. Ginger and H. Zeng, *Nat. Photonics*, 2020, **15**, 238–244.
11 L. Xu, J. Li, B. Cai, J. Song, F. Zhang, T. Fang and H. Zeng, *Nat. Commun.*, 2020, **11**, 3902.
12 Y. Jiang, C. Sun, J. Xu, S. Li, M. Cui, X. Fu, Y. Liu, Y. Liu, H. Wan, K. Wei, T. Zhou, W. Zhang, Y. Yang, J. Yang, C. Qin, S. Gao, J. Pan, Y. Liu, S. Hoogland, E. H. Sargent, J. Chen and M. Yuan, *Nature*, 2022, **612**, 679–684.
13 M. Ban, Y. Zou, J. P. H. Rivett, Y. Yang, T. H. Thomas, Y. Tan, T. Song, X. Gao, D. Credgington, F. Deschler, H. Sirringhaus and B. Sun, *Nat. Commun.*, 2018, **9**, 3892.
14 F. Zhang, H. Min, Y. Zhang, Z. Kuang, J. Wang, Z. Feng, K. Wen, L. Xu, C. Yang, H. Shi, C. Zhuo, N. Wang, J. Chang, W. Huang and J. Wang, *Adv. Mater.*, 2022, **34**, e2203180.
15 F. Yuan, X. Zheng, A. Johnston, Y. K. Wang, C. Zhou, Y. Dong, B. Chen, H. Chen, J. Z. Fan, G. Sharma, P. Li, Y. Gao, O. Voznyy, H. T. Kung, Z. H. Lu, O. M. Bakr and E. H. Sargent, *Sci. Adv.*, 2020, **6**, eabb0253.
16 J. Lu, X. Guan, Y. Li, K. Lin, W. Feng, Y. Zhao, C. Yan, M. Li, Y. Shen, X. Qin and Z. Wei, *Adv. Mater.*, 2021, **33**, e2104414.
17 D. Yang, G. Zhang, R. Lai, Y. Cheng, Y. Lian, M. Rao, D. Huo, D. Lan, B. Zhao and D. Di, *Nat. Commun.*, 2021, **12**, 4295.
18 Z. Ma, Z. Shi, C. Qin, M. Cui, D. Yang, X. Wang, L. Wang, X. Ji, X. Chen, J. Sun, D. Wu, Y. Zhang, X. J. Li, L. Zhang and C. Shan, *ACS Nano*, 2020, **14**, 4475–4486.
19 H. Chen, L. Zhu, C. Xue, P. Liu, X. Du, K. Wen, H. Zhang, L. Xu, C. Xiang, C. Lin, M. Qin, J. Zhang, T. Jiang, C. Yi, L. Cheng, C. Zhang, P. Yang, M. Niu, W. Xu, J. Lai, Y. Cao, J. Chang, H. Tian, Y. Jin, X. Lu, L. Jiang, N. Wang, W. Huang and J. Wang, *Nat. Commun.*, 2021, **12**, 1421.
20 A. Singh, N. C. Chiu, K. M. Boopathi, Y. J. Lu, A. Mohapatra, G. Li, Y. F. Chen, T. F. Guo and C. W. Chu, *ACS Appl. Mater. Interfaces*, 2019, **11**, 35088–35094.
21 M. Leng, Z. Chen, Y. Yang, Z. Li, K. Zeng, K. Li, G. Niu, Y. He, Q. Zhou and J. Tang, *Angew. Chem., Int. Ed.*, 2016, **55**, 15012–15016.
22 S. Gu, R. Lin, Q. Han, Y. Gao, H. Tan and J. Zhu, *Adv. Mater.*, 2020, **32**, e1907392.
23 M. Awais, R. L. Kirsch, V. Yeddu and M. I. Saidaminov, *ACS Mater. Lett.*, 2021, **3**, 299–307.
24 X. Jiang, Z. Zang, Y. Zhou, H. Li, Q. Wei and Z. Ning, *Acc. Chem. Res.*, 2021, **2**, 210–219.
25 B. B. Yu, Z. Chen, Y. Zhu, Y. Wang, B. Han, G. Chen, X. Zhang, Z. Du and Z. He, *Adv. Mater.*, 2021, **33**, e2102055.
26 C. Sun, P. Yang, Z. Nan, C. Tian, Y. Cai, J. Chen, F. Qi, H. Tian, L. Xie, L. Meng and Z. Wei, *Adv. Mater.*, 2022, e2205603.

27 J. Wu, S. C. Liu, Z. Li, S. Wang, D. J. Xue, Y. Lin and J. S. Hu, *Natl. Sci. Rev.*, 2021, **8**, nwab047.
28 L. Gu, D. Li, L. Chao, H. Dong, W. Hui, T. Niu, C. Ran, Y. Xia, L. Song, Y. Chen and W. Huang, *Sol. RRL*, 2021, **5**, 2000672.
29 S. Shao, J. Liu, G. Portale, H.-H. Fang, G. R. Blake, G. H. ten Brink, L. J. A. Koster and M. A. Loi, *Adv. Energy Mater.*, 2018, **8**, 1702019.
30 L. Zhu, H. Cao, C. Xue, H. Zhang, M. Qin, J. Wang, K. Wen, Z. Fu, T. Jiang, L. Xu, Y. Zhang, Y. Cao, C. Tu, J. Zhang, D. Liu, G. Zhang, D. Kong, N. Fan, G. Li, C. Yi, Q. Peng, J. Chang, X. Lu, N. Wang, W. Huang and J. Wang, *Nat. Commun.*, 2021, **12**, 5081.
31 Y. Liao, H. Liu, W. Zhou, D. Yang, Y. Shang, Z. Shi, B. Li, X. Jiang, L. Zhang, L. N. Quan, R. Quintero-Bermudez, B. R. Sutherland, Q. Mi, E. H. Sargent and Z. Ning, *J. Am. Chem. Soc.*, 2017, **139**, 6693–6699.
32 Y. Hassan, J. H. Park, M. L. Crawford, A. Sadhanala, J. Lee, J. C. Sadighian, E. Mosconi, R. Shivanna, E. Radicchi, M. Jeong, C. Yang, H. Choi, S. H. Park, M. H. Song, F. De Angelis, C. Y. Wong, R. H. Friend, B. R. Lee and H. J. Snaith, *Nature*, 2021, **591**, 72–77.
33 S. Tian, C. Zou, R. Lai, C. Hsu, X. Cao, S. Xing, B. Zhao and D. Di, *J. Semicond.*, 2022, **43**, 050502.
34 J. Zhang, Z. Xiong and X. S. Zhao, *J. Mater. Chem.*, 2011, **21**, 3634–3640.
35 M. Šeruga, M. Metikoš-Huković, T. Valla, M. Milun, H. Hoffschultz and K. Wandelt, *J. Electroanal. Chem.*, 1996, **407**, 83–89.
36 H. Xu, Y. Jiang, T. He, S. Li, H. Wang, Y. Chen, M. Yuan and J. Chen, *Adv. Funct. Mater.*, 2019, **29**, 1807696.
37 P. Li, H. Dong, J. Xu, J. Chen, B. Jiao, X. Hou, J. Li and Z. Wu, *ACS Energy Lett.*, 2020, **5**, 2327–2334.
38 H. Dong, C. Ran, W. Gao, N. Sun, X. Liu, Y. Xia, Y. Chen and W. Huang, *Adv. Energy Mater.*, 2021, **12**, 2102213.
39 L. Lanzetta, T. Webb, N. Zibouche, X. Liang, D. Ding, G. Min, R. J. E. Westbrook, B. Gaggio, T. J. Macdonald, M. S. Islam and S. A. Haque, *Nat. Commun.*, 2021, **12**, 2853.
40 X. Meng, Y. Wang, J. Lin, X. Liu, X. He, J. Barbaud, T. Wu, T. Noda, X. Yang and L. Han, *Joule*, 2020, **4**, 902–912.
41 C. Ran, W. Gao, J. Li, J. Xi, L. Li, J. Dai, Y. Yang, X. Gao, H. Dong, B. Jiao, I. Spanopoulos, C. D. Malliakas, X. Hou, M. G. Kanatzidis and Z. Wu, *Joule*, 2019, **3**, 3072–3087.
42 F. Wang, X. Jiang, H. Chen, Y. Shang, H. Liu, J. Wei, W. Zhou, H. He, W. Liu and Z. Ning, *Joule*, 2018, **2**, 2732–2743.
43 J. Wang, C. Yang, H. Chen, M. Lv, T. Liu, H. Chen, D.-J. Xue, J.-S. Hu, L. Han, S. Yang and X. Meng, *ACS Energy Lett.*, 2023, 1590–1596, DOI: **10.1021/acsenergylett.2c02776**.
44 M. H. Kumar, S. Dharani, W. L. Leong, P. P. Boix, R. R. Prabhakar, T. Baikie, C. Shi, H. Ding, R. Ramesh, M. Asta, M. Graetzel, S. G. Mhaisalkar and N. Mathews, *Adv. Mater.*, 2014, **26**, 7122–7127.